The implementation of diffuse radiation shading computation in ESP-r

Joe Clarke, Energy Systems Research Unit, University of Strathclyde, Scotland

Abstract

Approaches to the modelling of irradiance and illuminance distribution within the ESP-r system, based on direct computation and co-operating programs respectively, are summarised. A recent extension to the projection-based, solar shading algorithm of the former approach – addressing diffuse beam shading quantification under realistic sky conditions – is described. The paper concludes with results from an example application of the extended algorithm to investigate the impact of diffuse shading on photovoltaic component power output.

1. Introduction

Low energy approaches to building design, such as daylight-responsive luminaire control and building-integrated photovoltaic (PV) components, require modelling methods to predict the illuminance and irradiance of internal/external building surfaces in a manner that takes due account of realistic sky conditions and complex shading effects. A requirement within integrated building performance simulation is to re-compute the radiation distribution at each simulation time step in order to represent the relationship between shading (intentional or otherwise) and the changes in the radiation distribution. Another requirement relates to control: the hourly weather data normally employed is incompatible, in its frequency, with the requirements of realistic control algorithms as applied to luminaire switching/dimming or PV component electronics to maintain output at the maximum power point. Since changes in shading effects and occupancy interactions are normally instantaneous, it is not possible to interpolate between hourly results.

Two approaches have previously been implemented in ESP-r at the time-step level: one based on co-operation between ESP-r and RADIANCE (Larson and Shakespeare 1998); the other based on the projection of façade/surrounding obstructions onto external and internal surfaces at angles representing the incoming radiation. The shading factors derived from the latter method are then utilised within an inter-reflection model to determine the irradiance distribution; hitherto only direct shading was considered. The former method is used (albeit infrequently) to evaluate the illumination of internal surfaces under typical conditions to assess visual comfort or, via a photocell, to switch artificial lighting as an energy efficiency measure. The latter method is used in all simulations to evaluate the irradiance distribution and hence the solar flux inputs to all model surfaces at each simulation time-step. While the former method is general, its computational intensity has hitherto rendered it unsuitable for the latter task.

In both cases the Perez anisotropic sky radiance distribution model (Perez *et al* 1993) is used in conjunction with measured global and diffuse horizontal solar irradiance time series. Several possibilities exist to obtain such data at high frequency, e.g. the European Luminous Climate Atlas (EC 1995) or the use of a probability density algorithm (Skartveit and Olseth 1992) to generate

high frequency data from hourly values. It is also possible to bypass the Perez model and impose measured inclined surface measurements on a simulation.

Section 2 summarises the co-operative approach and comments on the barriers to its application at the time-step level, while Section 3 describes the extension of the projection approach to include diffuse shading. Finally, Section 4 presents the results of a study to quantify the impact of diffuse shading on PV component power output.

2. Co-operative method

Potentially, at each simulation time-step, ESP-r initiates and controls a RADIANCE ray tracing simulation (Clarke *et al* 1998) by: (1) transferring data defining the current solar position, the irradiance level and building state; (2) generating a sky model; (3) re-building a scene model to accommodate building changes, e.g. blind positioning; and (4) controlling the RADIANCE simulation as a function of the purpose in hand, e.g. daylight utilisation or visual comfort assessment. The data returned by RADIANCE may then be displayed or input to an ESP-r luminaire controller. ESP-r offers the Hunt (1979) stochastic algorithm to determine the likelihood of occupants switching on lights on arrival. Explicit dimming control algorithms are also available for automatic control. For example, an *integral reset* controller will adjust the dimming level so that the photocell signal is kept at a constant reference value established from night-time photocell calibration. At each simulation time-step, the dimming level in the controller's dynamic range, f_d, is determined from

$$f_d = 1 - \frac{E_{ds}}{E_{es}}$$

where E_{ds} is the predicted daylight illuminance of the photocell (lux) and E_{es} the artificial lighting photocell signal obtained from night-time calibration (lux). Alternatively, a *closed loop proportional* controller will adjust the dimming level as a linear function of the difference between the photocell signal and the night-time reference level. In this case a day-time calibration must be performed to determine a linear control function slope, m, used to determine the dimming level:

$$m = \frac{E_{dw}}{E_{dw}.E_{es} - E_{ew}.E_{ds}}$$

$$f_d = \frac{1 + m(E_{ds} - E_{es})}{1 - m.E_{es}}$$

where E_{dw} is the time varying daylight illuminance at selected workplace control points during day-time calibration and E_{ew} the electric lighting illuminance at the same points during night-time calibration.

In use, the co-operative method is computationally demanding and is usually invoked prior to an energy simulation to establish time invariant daylight coefficients to allow estimation of the internal surface illuminance distribution at each energy simulation time step thereafter. With problems involving temporal shading adjustment this approach would not be acceptable and either the computational penalty of time-step co-operation must be accepted or a mechanism found to reduce the problem to a manageable number of discrete lighting-related scenarios for which daylight coefficient sets may be pre-computed.

Bourgeois *et al* (2006) addressed the issue of occupant interaction by developing a sub-hourly, occupancy-based control (SHOCC) model based on algorithms from Lightswitch 2002 (Reinhart 2004) for manual/automatic lighting and window blind control (note that while

SHOCC was prototyped within ESP-r, it has not yet progressed to a level of refinement where it is generally available as a selectable option). Its function is to track the actions of individual occupants thus avoiding the need to represent activities such as lighting/occupant heat gain and blind activation by prescribed profiles. While the approach may be readily applied to problems with routine occupancy patters (e.g. school classrooms), it is more problematic with complex environments (e.g. open plan offices) where population behaviour is complex and uncertain.

The issue of how to implement a simulation-based approach to daylight design has been addressed by Reinhart and Wienold (2011), who proposed a 'daylighting dashboard' based on co-operation between several analysis tools and providing support for the appraisal of solutions in terms of daylight utilisation, visual comfort and energy performance metrics. Significantly, the approach hints at the possibility of controlling the invocation of the lighting simulation component on the basis of occupant changes to the building model as a mechanism to reduce the overall computational burden without significant loss of realism.

3. Projection method

The estimation of solar irradiance distribution is automatically invoked in ESP-r at each simulation time-step and is principally governed by shading effects. To avoid the computational burden of the co-operative method, a direct projection algorithm was established; this section describes the method with emphasis on the recent addition of diffuse beam shading.

The geometry of an ESP-r building and obstructions model comprises a collection of planar polygons each defined as a list of vertices (*x y z*) ordered anticlockwise when viewed from the 'outside'. Consider the following summations applied to the vertices of an arbitrary polygon, *p*.

$$\left.\begin{aligned} XS_p &= \sum_{i=1}^{NV}\left(y_i z_j - z_i y_j\right) \\ YS_p &= \sum_{i=1}^{NV}\left(z_i x_j - x_i z_j\right) \\ ZS_p &= \sum_{i=1}^{NV}\left(x_i y_j - y_i x_j\right) \end{aligned}\right\} \begin{matrix} j = i+1 \\ j > NV; j = 1 \end{matrix}$$

where *NV* is the number of vertices in the polygon; the polygon area is then given by

$$A_p = 0.5\left(XS_p^2 + YS_p^2 + ZS_p^2\right)^{½}$$

and the perimeter length by

$$L_p = \sum_{i=1}^{NV}\left[\left(x_j - x_i\right)^2 + \left(y_j - y_i\right)^2 + \left(z_j - z_i\right)^2\right]^{½} \left.\begin{matrix} j = i+1 \\ j > NV; j = 1 \end{matrix}\right\}.$$

The surface azimuth may also be determined from the above summations:

$$\alpha_p = tan^{-1}\left(\frac{XS_p}{YS_p}\right)$$

where, for $YS_p = 0$,

$$\begin{aligned} \alpha_p &= -90^{\circ} \text{for } XS_p < 0 \\ \alpha_p &= \quad 0^{\circ} \text{for } XS_p = 0 \\ \alpha_p &= \quad 90^{\circ} \text{for } XS_p > 0 \end{aligned}$$

and the surface elevation from

$$\beta_p = tan^{-1}\left[\frac{ZS_p}{\left(XS_p^2 + YS_p^2\right)^{½}}\right]$$

where, for $XS_p^2 + YS_p^2 = 0$,

$$\beta_p = -90^{\circ} \text{for } ZS_p < 0$$
$$\beta_p = \quad 0^{\circ} \text{for } ZS_p = 0$$
$$\beta_p = \quad 90^{\circ} \text{for } ZS_p > 0.$$

Finally, the volume contained by a set of bounding polygons is evaluated as the algebraic summation of the volumes of prisms formed by connecting the vertices of each surface to the origin of the coordinate system:

$$V = \frac{1}{6}\sum_{j=1}^{NP}\left(x_{j1}XS_j + y_{j1}YS_j + z_{j1}ZS_j\right)$$

where $\left(x_{j1}\ y_{j1}\ z_{j1}\right)$ are the co-ordinates of vertex *1* in polygon *j* and *NP* the total number of polygons (zone surfaces).

The irradiance distribution algorithm uses these parameters to evaluate the time varying solar shading of the external and internal surfaces of the target building as a function of façade, surrounding and internal obstructions, each of which may have an opacity factor less than unity. This is done separately for the direct and diffuse radiation components (typically from a regular anisotropic sky although real skies may be imposed). The algorithm proceeds as follows for each time instance and target surface.

1) Mesh the external or internal target surface.
2) Determine the solar azimuth and altitude angles relative to the site coordinate system.
3) Abandon the calculation for the current time step is before sunrise or after sunset.
4) For each obstruction surface:
   a) project the surface (where a projected surface crosses the plane of the target surface, the intersection points are located and used in place of the yon-side points);
   b) test each target surface mesh cell's centre point to determine if it is contained by the projected shadow polygon;
   c) summate contributions to each mesh cell for all obstructions taking account of opacities;
   d) repeat from step a) for all sky patches representing the discretised sky.
5) Iterate from 1) until all target surfaces are processed.

Starting with a collection of target and obstruction surfaces expressed relative to an arbitrary *XYZ* site co-ordinate system, the vertical *XZ* plane is relocated to the plane of each target surface in turn. This allows the surface shading to be determined from rudimentary two-dimensional operations; this is achieved by applying a transformation equation for translation and 3D rotation as given below.

A mesh is superimposed on the target surface to enable testing for overlap with individual shadow polygons associated with façade, surrounding and internal solar obstructions. Each obstruction surface is projected onto the target surface at an angle that corresponds to a particular sky patch of known directionality (azimuth and altitude angle). The default sky discretisation scheme comprises 145 patches although this may be varied: up for more accuracy, down for faster computation. This discretisation, along with the resolution of the target surface mesh, both of which are under definable, controls the final accuracy of the approach. Where a patch defines the

current solar position, the outcome represents direct beam shading. Otherwise, the integration of all patches represents diffuse radiation shading. By extending the number of patches that represent the current solar position, the directionality of the circumsolar component may be explicitly represented. The projected obstruction surface for each sky patch is a two-dimensional polygon expressed relative to the local target surface co-ordinate system and is achieved by application of the following translation, rotation and projection transformation equation. In this equation, the projection angles are pseudo solar angles in that the actual patch azimuth and elevation angles are expressed relative to the local target surface's coordinate system. These pseudo angles are established by firstly transforming the incidence vector to the local co-ordinate system by applying the following equation but without the projection terms.

$$\begin{aligned} x_p = {} & x_T \cos\gamma \cos\alpha + \sin\beta \sin\gamma \cos\alpha - z_T \cos\beta \sin\gamma \cos\alpha + y_T \cos\beta \sin\alpha + z_T \sin\beta \sin\alpha \\ & - x_T \cos\gamma \sin\alpha (\pm \tan\xi_1) - y_T \sin\beta \sin\gamma \sin\alpha (\pm \tan\xi_1) \\ & + z_T \cos\beta \sin\gamma \sin\alpha (\pm \tan\xi_1) + y_T \cos\beta \cos\alpha (\pm \tan\xi_1) \\ & + z_T \sin\beta \cos\alpha (\pm \tan\xi_1) \end{aligned}$$

$$\begin{aligned} y_p = {} & -x_T \cos\gamma \sin\alpha - y_T \sin\beta \sin\gamma \sin\alpha + z_T \cos\beta \sin\gamma \sin\alpha + y_T \cos\beta \cos\alpha \\ & + z_T \sin\beta \cos\alpha \end{aligned}$$

$$\begin{aligned} z_p = {} & -x_T \cos\gamma \sin\alpha \left(\pm \frac{\tan\xi_2}{\cos\xi_1}\right) - y_T \sin\beta \sin\gamma \sin\alpha \left(\pm \frac{\tan\xi_2}{\cos\xi_1}\right) \\ & + z_T \cos\beta \sin\gamma \sin\alpha \left(\pm \frac{\tan\xi_2}{\cos\xi_1}\right) + y_T \cos\beta \cos\alpha \left(\pm \frac{\tan\xi_2}{\cos\xi_1}\right) \\ & + z_T \sin\beta \cos\alpha \left(\pm \frac{\tan\xi_2}{\cos\xi_1}\right) + x_T \sin\gamma - y_T \sin\beta \cos\gamma + z_T \cos\beta \cos\gamma \end{aligned}$$

The computation for the current obstruction surface is abandoned if it is entirely on the yon-side of the target surface relative to the sky patch and therefore cannot cause shading, or the transformed surface (translation and rotation only) faces away from the sky patch and therefore cannot be irradiated. Where the obstruction surface crosses the plane of the target surface, the intersection points are determined and used in place of the yon-side points in the above projection.

Point containment tests are now initiated to determine which building surface mesh cells are within a given projected shadow polygon; all 'hits' to a mesh cell are recorded separately for the direct and diffuse radiation components. At the start of a time step, each cell is assigned a value of 0 to indicate that it is fully insolated; any cell contained by a shadow polygon is then reassigned a non-zero value constrained to a maximum of unity. Point containment is established by radiating a line away from the centroid of the cell in an arbitrary direction. If the number of intersections with the co-planar shadow polygon is odd, the point is contained. The merit of the method, besides its relative rapidity, is that it allows both magnitude and point of application estimation, with accuracy (and computation speed) controlled by simply varying the grid size.

The total direct or diffuse shading factor, S_t, for a target surface mesh cell at some point in time is obtained as the summation of all projected obstruction block surfaces that contain the cell:

$$S_t = \sum_{i=1}^{NS} 1 - (1 - S_{i-1})(1 - O_i)\,;\; 0 \geq S_I \leq 1$$

where *NS* is the number of obstruction surfaces in question, S_i the shadow factor contribution (proportion of one, S_0 initialised to zero) and *O* the opacity of an obstruction surface (proportion of one). When S_t attains a value of unity, the remaining obstruction surface projections are abandoned because the target surface cell is then fully shaded for the current sky patch (this will occur after

encountering the first shadow polygon if its parent obstruction is opaque). This device results in a significant reduction in the computational load.

The time varying grid cell shading factors are applied, as appropriate, to the sky patch irradiance and the outcome input to ESP-r's radiation distribution model to obtain the radiation injections to internal and external surfaces (after window transmission and intra-zone multiple reflections in the former case) – and intra-constructional nodes in the case of partly transparent constructions such as a PV façade.

To date, the performance of the extended algorithm has been confirmed by using ESP-r's shadow display facility to visualise sky patch obscuration by obstructions, with the result compared to the computed shadow factor. A direct inter-comparison with RADIANCE predictions is underway.

Overall, the method is fast relative to the co-operative approach, with the computational burden no greater that that required for the other technical domains comprising the integrated building model. For example, on a processor using the Intel Atom™ chipset with 1 GB memory, a simulation running within a Linux Guest Operating System, with shading computation at each time step, took 57% longer than a simulation with pre-computed shading factors. This may be contrasted to the co-operative method where the lighting simulation can be 2-3 orders of magnitude greater that the energy simulation (and in some cases considerable more).

4. PV diffuse shading sensitivity

Consider an example application of the extended projection method to the case of a PV façade with the aim of assessing the impact of omitting consideration of diffuse radiation shading: while it may reasonably be assumed that best practice design will not permit direct beam shading, this is unlikely to be the case for the diffuse beam due to skyline obstruction of the sky vault caused by natural features and surrounding built forms. Consider the application of 2 polycrystalline PV modules to a South-facing building façade with opaque skyline obstructions obscuring 0%, 10%, 20% and 40% of the sky vault but positioned to give rise to zero direct shading. Each module has a nominal maximum power of 80 W and the power output is proportional to the non-shaded irradiation area. Figures 1 and 2 present ESP-r simulation results over typical days in Spring and Summer for a UK climate.

In Spring, and with no direct or diffuse shading, the PV generates some 839 Wh over the typical day. This output falls by 11.8% (to 740 Wh), 15.7% (to 707 Wh) and 32.5% (to 566 Wh) for the 10%, 20% and 40% obscured skyline cases respectively. In Summer, with no direct or diffuse shading, the PV generates 786 Wh over the typical day, falling by 14.2% (to 674 Wh), 19% (to 636 Wh) and 37.2% (to 494 Wh) for the 10%, 20% and 40% obscured skyline cases respectively. The 3 obscuration values correspond to predicted diffuse shading factors of approximately 21.2%, 28.4% and 55.7% respectively; here time invariant because the sky luminance distribution function does not change with time.

Such results indicate a significant impact of diffuse shading; a finding that vindicates the integrated simulation approach as an apt means to both accurately size renewable energy components and assess their performance under realistic operating conditions.

To verify the new algorithm, the ESP-r predictions were compared with corresponding values determined from RADIANCE simulations and close agreement was observed in all cases: for example, the comparable value for the 40% skyline obscuration case was 56% (i.e. 0.5%

higher). This comparable value was obtained from a RADIANCE simulation with no reflections from the ground or skyline obstructions, which is appropriate here because the diffuse shading factors are separately applied within ESP-r to obtain the externally reflected component of the total surface solar irradiation.

5. Conclusion

Integrated building performance modelling provides a means to represent all relevant aspects of a problem to an adequate level of realism. At the present state-of-the-art, some domains require significant computational effort and this gives rise to the need for simplifications where applicable. This paper has demonstrated such a simplification in relation to the repetitive computation of direct and diffuse shading throughout a simulation. The technique is relatively fast with no significant loss of accuracy and is able to accommodate realistic sky types and time varying changes to the building model as might occur due to control action or occupancy behaviour.

Through simulations incorporating the technique, it has been demonstrated that the omission of diffuse shading will result in an optimistic prediction of PV component power output.

6. References

Bourgeois D, Reinhart C and MacDonald I (2006) 'Adding advanced behavioural models in whole building energy simulation: A study on the total energy impact of manual and automated lighting control', *Energy and Buildings*, 38, pp814-823.

Clarke J A, Janak M and Ruyssevelt P (1998) 'Assessing the overall performance of advanced glazing systems', *Solar Energy*, V63 (1), pp231-41.

Hunt D R G (1979) 'The use of artificial lighting in relation to daylight levels and occupancy', *Building and Environment*, 14, pp21-33.

Larson G W and Shakespeare R (1998) *Rendering with Radiance - The Art and Science of Lighting Visualization*, Morgan Kaufmann.

Reinhart C F and Wienold J (2011) 'The daylighting dashboard – A simulation-based design analysis for daylit spaces', *Building and Environment*, 46, pp386-396.

Reinhart C F (2004) 'Lightswitch 2002: a model for manual control of electric lighting and blinds', *Solar Energy*, 77(1), pp15-28.

Perez R, Seals R and Michalsky J (1993) 'All-weather model for sky luminance distribution - preliminary configuration and validation', *Solar Energy*, 50(3), pp235-253.

EC (1995) 'European luminous climate atlas', *Final report for JOU2-CT920144 CIPD-CT 925033*.

Skartveit A and Olseth J A (1992) 'The probability density and autocorrelation of short-term global and beam irradiance' *Solar Energy*, 49(6), pp477-487.

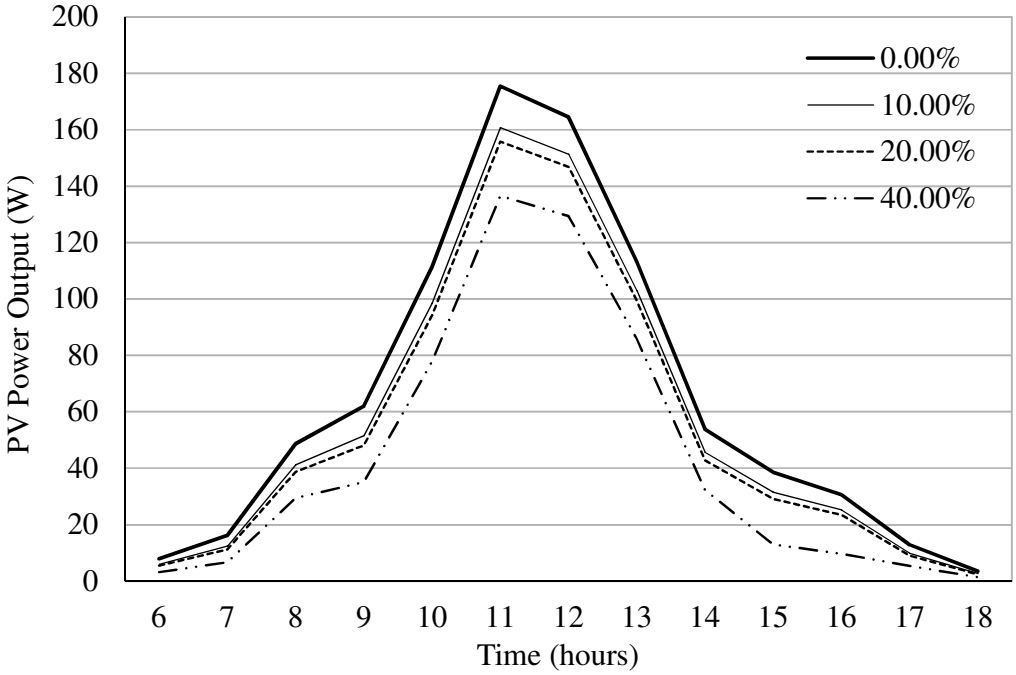

Figure 1: PV power output for various skyline obscuration extents – Spring typical day, UK climate.

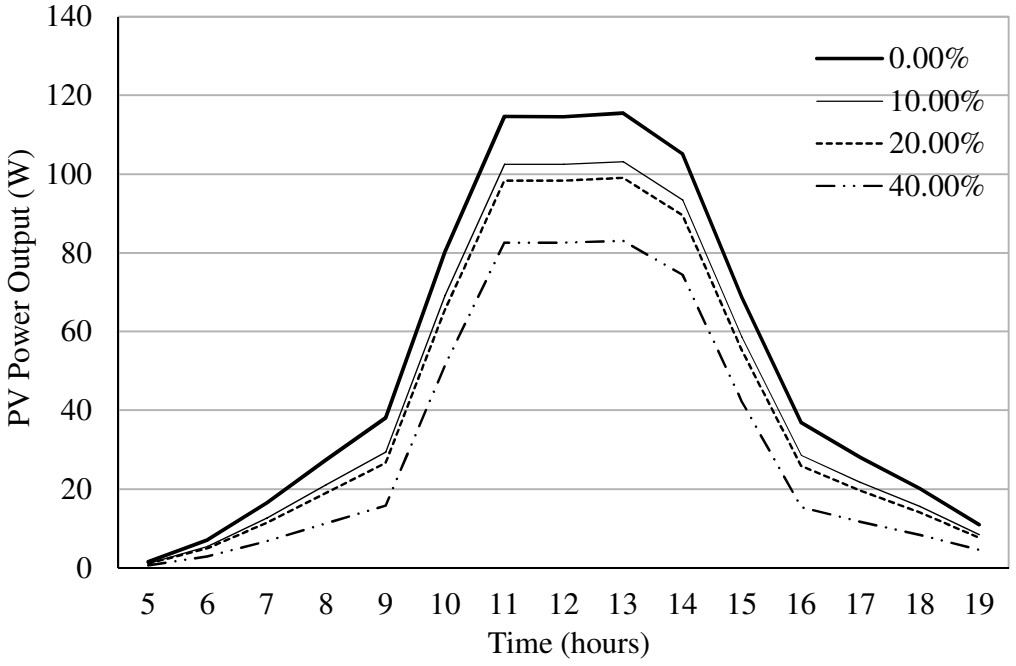

Figure 2: PV power output for various skyline obscuration extents – Summer typical day, UK climate.